Ab initio configuration interaction study of the *B*- and *C*-band photodissociation of methyl iodide

Cite as: J. Chem. Phys. **134**, 044303 (2011); https://doi.org/10.1063/1.3532926
Submitted: 15 October 2010 . Accepted: 08 December 2010 . Published Online: 25 January 2011

Aleksey B. Alekseyev, Heinz-Peter Liebermann, and Robert J. Buenker

Ab initio configuration interaction study of the *B*- and *C*-band photodissociation of methyl iodide

Aleksey B. Alekseyev,[a] Heinz-Peter Liebermann, and Robert J. Buenker
Fachbereich C, Theoretische Chemie, Bergische Universität Wuppertal, Gaußstr. 20, D-42097 Wuppertal, Germany

(Received 15 October 2010; accepted 8 December 2010; published online 25 January 2011)

Multireference spin–orbit configuration interaction calculations have been carried out for the valence and low-lying Rydberg states of CH_3I. Potential energy surfaces along the C–I dissociation coordinate (minimal energy paths with respect to the umbrella angle) have been obtained as well as transition moments for excitation of the Rydberg states. It is shown that the B and C absorption bands of CH_3I are dominated by the perpendicular $^3R_1$, $^1R(E) \leftarrow \tilde{X}\,A_1$ transitions, while the $^3R_2(E)$, $^3R_{0^+}(A_1) \leftarrow \tilde{X}\,A_1$ transitions are very weak. It is demonstrated that the bound Rydberg states of the B and C bands are predissociated due to the interaction with the repulsive E and A_2 components of the $^3A_1$ state, with the $^3A_1(E)$ state being the main decay channel. It is predicted that the only possibility to obtain the $I(^2P_{3/2})$ ground state atoms from the CH_3I photodissociation in the B band is by interaction of the $^3R_1(E)$ state with the repulsive $^1Q(E)$ valence state at excitation energies above 55 000 cm^{-1}. The calculated *ab initio* data are used to analyze the influence of the Rydberg state vibrational excitation on the decay process. It is shown that, in contrast to intuition, excitation of the ν_3 C–I stretching mode supresses the predissociation, whereas the ν_6 rocking vibration enhances the predissociation rate. © *2011 American Institute of Physics*. [doi:10.1063/1.3532926]

I. INTRODUCTION

The CH_3I photodecay in its first absorption continuum (A band) serves as a benchmark process for analysis of the multichannel photodissociation of polyatomic molecules, and an enormous amount of work has been done to describe this process (see Refs. 1–5 and references therein). Much less is known, however, for the next UV absorption bands of CH_3I, the B and C bands, and what information is available comes mainly from experiment. In our recent methyl iodide studies,[4,5] we have carried out the *ab initio* calculations of potential energy surfaces (PESs) and transition moments for the low-lying valence states and on this basis performed a detailed analysis of the CH_3I photodissociation in the A band. In the present work, we extend such *ab initio* analysis to the B and C bands of CH_3I and attempt to answer a number of open questions concerning CH_3I photodissociation in this excitation range.

The CH_3I absorption in the B and C bands is characterized by transitions to bound Rydberg states, followed by their prompt predissociation into the $CH_3(^2A_2'') + I(^2P_{1/2}), I(^2P_{3/2})$ products. Hereafter, the $I(^2P_{3/2})$ ground state atom is denoted as I, whereas the spin-excited $I(^2P_{1/2})$ atom is called I^*. Similar to the A band case, the product branching ratio $\Gamma(\lambda) = [I^*]/[I]+[I^*]$ remains a key characteristic of the CH_3I photodissociation in the B and C bands. Since no other decay channels are relevant to the problem discussed, this quantity is also quite often called the I^* quantum yield and denoted as $\Phi_{I^*}(\lambda)$.

The absorption spectra for the B and C bands have been measured and analyzed.[6,7] A number of vibrational levels in the upper electronic states have been assigned[6,8] and predissociation-mediated excited state lifetimes have been determined.[8] A variety of different experimental approaches have been used to probe the CH_3I photodecay products in the B and C bands, including time-of-flight mass-spectrometry,[9–11] Raman spectroscopy,[12] femtosecond photoionization spectroscopy,[8,13] multiphoton ionization detection in combination with velocity map imaging,[14] and time-resolved photoelectron spectroscopy.[15]

Hess *et al.*[16] have probed the atomic iodine photofragment employing the diode laser gain versus absorption method at an excitation wavelength of 193 nm and obtained $\Gamma = 0.70 \pm 0.04$. This result is in strong contradiction, however, with the measurements of van Veen *et al.*[9] and Continetti *et al.*,[10] who determined the branching ratio to be unity at the same wavelength. Recently, Gilchrist *et al.*[17] have reexamined the CH_3I photodissociation in the B band by employing two different diode laser techniques. Frequency-modulated diode laser based absorption spectroscopy has been used to extract nascent Doppler lineshapes from which a branching ratio of unity has been obtained at $\lambda = 193$ nm. This result confirms the earlier finding of Refs. 9 and 10. However, the diode laser gain/absorption measurements carried out in the same study gave $\Gamma = 0.68 \pm 0.04$.[17] The authors have concluded that the results of the diode laser gain/absorption measurements are distorted due to the formation of molecular iodine which dissociates to produce both the I and I^* atoms. This effect leads to a decrease of the measured Γ values in such experiments. From the above discussion it is clear that an important goal of the *ab initio* calculations must be to analyze whether the

[a]Author to whom correspondence should be addressed. Electronic mail: alexeev@uni-wuppertal.de.

formation of the ground state I atoms in the B band photofragmentation of CH_3I is at all possible and, if so, under which conditions.

The very recent femtosecond pump–probe experiment with velocity map imaging reported by Gitzinger *et al.*[14] provides a detailed picture of real-time predissociation in the B-band origin at 201.2 nm. This study confirms the iodine branching ratio to be unity and shows that the main channels which are open upon excitation in the band origin are $I(^2P_{1/2})$ + $CH_3(\nu_1 = 0, 1; \nu_2 = 0, 1, 2)$. A value of 1.5 ± 0.1 ps determined for the predissociation lifetime of the excited state agrees very well with the earlier result of 1.38 ± 0.14 ps obtained by Baronavski and Owrutsky.[8] The time-resolved measurement of the angular anisotropy of the dissociation products confirms both (i) the purely perpendicular nature of the B-band transition and (ii) the significant loss of anisotropy due to the CH_3I rotation during the lifetime of the excited state.

The B band of methyl iodide covers the spectral range from 190 to 205 nm and results from excitation of the lone-pair $e(5p_{x,y})$ electron located on the I atom to the $a_1(6s)$ Rydberg orbital. This excitation produces the $^{3,1}E$ states ($^{3,1}\Pi$ in the $C_{\infty v}$ group notation), where the triplet state is strongly split due to the spin–orbit (SO) interaction. The latter is stronger than the exchange interaction in this case, which leads to the formation of the two "doublet" pairs: $\{E(^3\Pi_2), E(^3\Pi_1)\}$ and $\{A_1(^3\Pi_0), E(^1\Pi)\}$, rather than to the conventional triplet + singlet combination typical for weak SO coupling. Absorption to these four states is somewhat artificially divided into two bands, B and C, where transitions to the two lower states are traditionally considered as belonging to the B band, while transitions to the upper two form the higher-lying C band (170–185 nm).

Donaldson *et al.*[18] have reported calculations of the predissociation dynamics for the low-lying Rydberg states. These calculations are based on the empirical PESs for the bound potentials plus a combination of early experimental and theoretical[19] data for the dissociative surfaces. The authors have also made a number of additional empirical assumptions concerning the coupling of PESs involved in the dissociation process. Their model has led to a prediction that at least two dissociative potentials (of A_1 and A_2 symmetries) are important for predissociation of the B-band states. Based on the data of Refs. 18 and 19, Syage[11] has concluded that the A_2 component of the repulsive $^3Q_0$ state belonging to the A band is responsible for the predissociation of the B and C states. Wang *et al.*[20] have also used this assumption in their recent experimental study to explain the B-band predissociation of CH_3I, having assumed, in addition, that a second crossing between the $^3Q_0$ and ^1Q states plays an important role. The above assumptions should be verified based on the new and more detailed *ab initio* calculations.

To the best of our knowledge, no *ab initio* data for the methyl iodide Rydberg states are available, with the exception of the early study of Tadjeddine *et al.*[19] and our CH_3I calculations[4] that deal primarily with the A band. The goal of the present study is to obtain the required *ab initio* data and to analyze the CH_3I predissociation in its B and C bands on this basis.

II. DETAILS OF THE COMPUTATIONAL METHOD

The present calculations of the methyl iodide Rydberg states are based on the experience of our recent calculations of the A-band valence states of this molecule[4,5] and are carried out in a similar way. Some adjustment of the configuration interaction (CI) treatment (reference and selected CI spaces, numbers of roots per $\Lambda - S$ symmetry) might be necessary in order to improve the description of the Rydberg states. Test calculations have been carried out at a number of representative geometries to find out which changes in the CI calculations should be done.

As in the previous studies,[4,5,21] the core electrons of the iodine atom are described by a relativistic effective core potential (RECP) given by LaJohn *et al.*[22] which includes all but the outer $5s$ and $5p$ electrons treated explicitly via basis functions. The original RECP SO operator for the I atom[22] has been scaled in this study with a factor of 1.05, which improves agreement with the $I(^2P_{1/2} - {}^2P_{3/2})$ atomic SO splitting of 7603 cm^{-1} (see Ref. 4).

The atomic orbital (AO) basis set for the I atom is the same as employed in our previous calculations of the iodine-containing molecules[4,21] and is adapted from the all-electron Cartesian Gaussian set of Glukhovtsev *et al.*[23] It is a $(7s7p3d1f)$ fully uncontracted set, described in more detail in our earlier work.[21] The test calculations performed in the present study have shown that diffuse s and p orbitals contained in this set are sufficient to describe the lowest Rydberg states of CH_3I, which allows one to avoid unnecessary enlargement of the I atomic basis. The AO basis for the C atom is the $(10s5p2d1f)/[4s3p2d1f]$ correlation consistent triple-zeta (cc–pVTZ) set, whereas for the hydrogen atom the $(5s2p1d)/[3s2p1d]$ set of the same type has been employed, both constructed by Dunning.[24]

The first step in the present theoretical treatment of the CH_3I molecule is a self-consistent-field (SCF) calculation of the $\tilde{X}^1A_1(...a_1^2e^4)$ closed-shell ground state, where the C_{3v} point group notation is used for molecular orbitals (MOs). All computations are carried out in the C_s symmetry group, which is the highest order Abelian subgroup of C_{3v} (the CI package employed treats only Abelian groups). The correspondence between C_{3v} and C_s groups is very simple: the a_1 irreducible representation (IR) in C_{3v} corresponds to a' in C_s, a_2 to a'', and e is split into $a' + a''$.

The next step is to carry out a series of multireference single- and double-excitation CI calculations for several lowest roots of each $\Lambda - S$ symmetry. At this stage of the calculations the SO interaction is neglected, but other relativistic effects are included through the spin-independent part of the iodine RECP. Results are obtained in the R_{C-I} distance interval from 3.4 to 10.0 a_0, with an increment of 0.05–0.10 a_0 in the Franck–Condon (FC) region (3.4–5.0 a_0) and with a larger increment at longer distances. Since the CH_3 radical is planar, there is one more coordinate which exhibits great changes in the CH_3I photodissociation process, namely the umbrella angle $\alpha = \angle$ H–C–H. To obtain the minimal energy path energies for the ground and excited states with respect to α, the umbrella angle has been varied in a small interval around the approximate equilibrium α values obtained for the two lowest

TABLE I. Technical details of the LSC–SO–CI calculations in C_s symmetry at $T = 0.25 \mu E_h$.[a]

C_s IR	N_{root}	N_{ref}	SAFTOT	SAFSEL	C_{3v}
$^1A'$	6	85	23 336 441	404 594	$^1A_1$, ^1E
$^1A''$	5	95	31 812 753	403 962	$^1A_2$, ^1E
$^3A'$	5	88	42 997 664	556 845	$^3A_1$, ^3E
$^3A''$	5	95	58 550 687	492 916	$^3A_2$, ^3E

[a]SAFTOT designates the total number of generated spin-adapted functions (SAF), SAFSEL designates the number of selected SAFs, and N_{ref} and N_{root} refer to the number of reference configurations and roots treated, respectively. The numbers of selected SAFs are given for $R_{C-I} = 4.04\ a_0$ and $\alpha = 111.0°$.

Rydberg states in our earlier study.[4] To minimize the scope of the calculations, no variations of the bending angle β or R_{C-H} bond lengths have been carried out.

Numbers of roots treated and reference configurations are given in Table I along with the numbers of generated and selected configurations, the latter giving the orders of the secular equations to be solved explicitly. The CI calculations are carried out with a standard perturbative selection procedure[25] for a threshold of $T = 0.25\ \mu E_h$. The Table–CI algorithm[26] is employed to compute Hamiltonian matrix elements between the many-electron basis functions, and a Direct-CI technique[27] is used to obtain the energy eigenvalues and eigenvectors for various $\Lambda - S$ states. The generalized multireference Davidson correction[28,29] is also applied for each root in order to estimate the effect of higher excitations on the computed energies.

In this study, we employ the same computational approach for including SO coupling, as used before in Ref. 4. It involves forming a matrix representation of the full relativistic Hamiltonian on the basis of the $\Lambda - S$ wave functions and can be viewed as a CI method employing a heavily contracted many-electron basis ($\Lambda - S$ contracted SO–CI or simply LSC–SO–CI (Ref. 30)), though with spin–orbit interaction instead of Coulomb and exchange terms as nondiagonal matrix elements. The above computations have been used to obtain all valence electronic states as well as the low-lying Rydberg states, transitions to which are responsible for the B and C absorption bands of the CH_3I molecule. The main difference of the present calculations in comparison with our earlier CH_3I study[4] lies in a larger number of calculated $^1A'$ and $^1A''$ roots and as a consequence in significantly larger CI spaces treated explicitly in these symmetries.

Our earlier HI and CH_3I studies[5,21] have shown that accurate calculations of the relevant transition moments require inclusion of a large number of higher-lying $\Lambda - S$ states, whose influence on the computed energies is practically negligible but whose contributions to the relatively weak spin-forbidden transitions are essential. Therefore, to obtain transition moments for the B- and C-band states, an additional series of LSC–SO–CI calculations has been carried out in which a significantly larger number of roots (17–18 roots for each of the $^{1,3}A'$, $^{1,3}A''$ IRs) have been obtained and the resulting SO matrix has been diagonalized. The test calculations have indicated that a further increase of the root number to 22–24 does not lead to significant changes in the computed transition moment values. The CI reference spaces in the extended LSC–SO–CI calculations contain 331–351 spin-adapted functions (SAFs), and the calculations have been carried out with a selection threshold of $T = 0.8\ \mu E_h$, a slight improvement in comparison to our previous study.[5] The orders of the secular equations (selected SAFs) lie in the $(3.3 - 6.4) \times 10^5$ range depending on the $\Lambda - S$ symmetry and molecular geometry.

III. RESULTS AND DISCUSSION

A. Potential energy surfaces along the C–I stretch coordinate

The calculated PESs for the lowest valence and Rydberg states are shown in Fig. 1 as functions of the C–I coordinate. These are the minimal energy paths with respect to the umbrella angle α for all states presented, i.e., they have been separately minimized by varying the α angle for every C–I distance and every state. One should note that although the $\Lambda - S$ notation (^3Q, $^3A_1$, etc.) is used for brevity in this figure, the states have been calculated including the SO interaction. We also employ here the $^{1,3}R$ notation for the lowest Rydberg states, which is an extension of Mulliken's $^{1,3}Q$ notation for the A-band states and indicates their close similarity to the $^{1,3}\Pi$ Rydberg states in isovalent $C_{\infty v}$ molecules such as diatomic hydrogen halides.

The lowest valence states, $^3Q(E, E, A_2, A_1)$ and $^1Q(E)$, where the C_{3v} double group notation is given in parentheses, arise from the $n(e) \rightarrow a_1^*$ (lone-pair to antibonding) orbital excitation and have strongly repulsive PESs

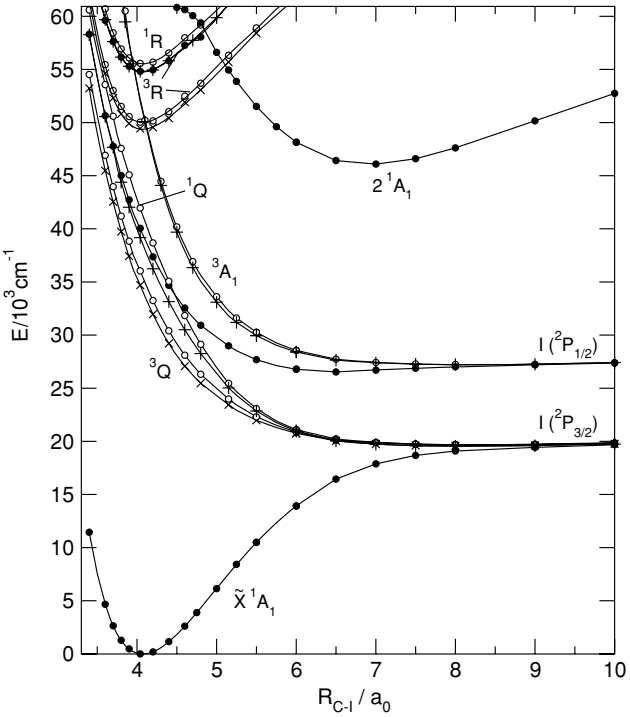

FIG. 1. Computed potential energy curves along the R_{C-I} stretch coordinate for the low-lying states of CH_3I: A_1 states—filled circles, A_2 states—pluses, and E states—open circles and crosses (C_{3v} group notation). Crosses correspond to the $\Omega = 2$ states in the $C_{\infty v}$ group, open circles to $\Omega = 1$. The $\Lambda - S$ notation (^3Q, ^3R, $^3A_1$) designates groups of the SO split states.

along the C–I coordinate in the FC region. Transitions to the $^3Q_{0^+}$,^1Q, and $^3Q_1$ states are responsible for the unresolved Gaussian-type absorption continuum called the A band. Four of the $^{3,1}Q$ states converge to the lowest $CH_3(^2A_2'')$ + $I(^2P_{3/2})$ dissociation limit, while $^3Q_{0^+}(A_1)$ goes to the $CH_3(^2A_2'')$ + $I(^2P_{1/2})$ asymptote lying 7603 cm^{-1} higher. The $^3Q_{0^+}$ state possesses a shallow potential minimum of 850 cm^{-1} at $R_{C-I} = 6.5\ a_0$. The energy and radiative properties of the A-band states as well as the CH_3I photodissociation process in this energy range have been described in great detail in our earlier studies.[4,5]

The next two valence states are the A_2 and E components of the $^3A_1$ state and they lie notably higher as can be expected from their $a_1 \rightarrow a_1^*$ (bonding to antibonding) origin. The $^3A_1$ splitting is relatively small due to the essentially Σ character of this state which corresponds to $^3\Sigma^+$ in $C_{\infty v}$. The $^3A_1$ splitting is 160 cm^{-1} at $R_{C-I} = 4.1\ a_0$ and increases up to 570 cm^{-1} at 4.8 a_0 before vanishing at the dissociation limit, where both the A_2 and E states converge to the same $I(^2P_{1/2})$ asymptote. At $R_{C-I} \geq 4.1\ a_0$, the $^3A_1$ splitting is mainly caused by a second-order SO interaction with the $^1Q(E)$ state which pushes $^3A_1(E)$ above the $^3A_1(A_2)$ component, but at shorter C–I distances SO coupling with the Rydberg states comes into play and the $A_2 - E$ splitting becomes less regular. Transition to the $^3A_1(E)$ state gives a contribution to the A absorption band in its blue tail above 47×10^3 cm^{-1}; but as has been shown in our previous study,[5] it is very weak.

There is one more valence state, $2\,^1A_1(A_1)$, which arises from the same $a_1 \rightarrow a_1^*$ excitation as $^3A_1$, but lies significantly higher than the latter in the FC region. At large C–I internuclear separations, this state converges to the excited CH_3 asymptote lying much higher in energy, which leads to a minimum on the $2\,^1A_1$ PES at $R \approx 7.0\ a_0$. This state has not yet been observed experimentally because of the very unfavorable FC factors. It might be responsible for depopulation of the lowest Rydberg states, though only in combination with relatively high vibrational excitation of the latter. It is worth noting that the present calculations have been extended in their CI part to improve the description of the low-lying Rydberg states. This does not lead to any significant changes in the results for the valence states, so that all previous conclusions concerning the A band are unchanged.

The lowest Rydberg states of CH_3I correspond to the $n(5p^I_{x,y}) \rightarrow 6s_I$ excitation and appear at energies around 5×10^4 cm^{-1}. Their PESs are enlarged in Fig. 2 together with those for the repulsive valence states which can be relevant to the Rydberg state predissociation. One can clearly see two pairs of Rydberg states, ($^3R_2$, $^3R_1$) and ($^3R_0$, ^1R), responsible for the B and C absorption bands, respectively. Both lower states as well as ^1R transform according to the E IR of the C_{3v} double group, but subscripts 2 and 1, which denote approximate Ω values, are useful for understanding possible strengths of the corresponding transitions. The upper group, in fact, consists of three states, since $^3R_0$ is split into the $0^+(A_1)$ and $0^-(A_2)$ components due to second-order SO interaction. This $0^+ - 0^-$ splitting is very small, only a couple of wavenumbers in the FC region, and becomes slightly larger in the region of a conical intersection with the $2\,^1A_1$ state.

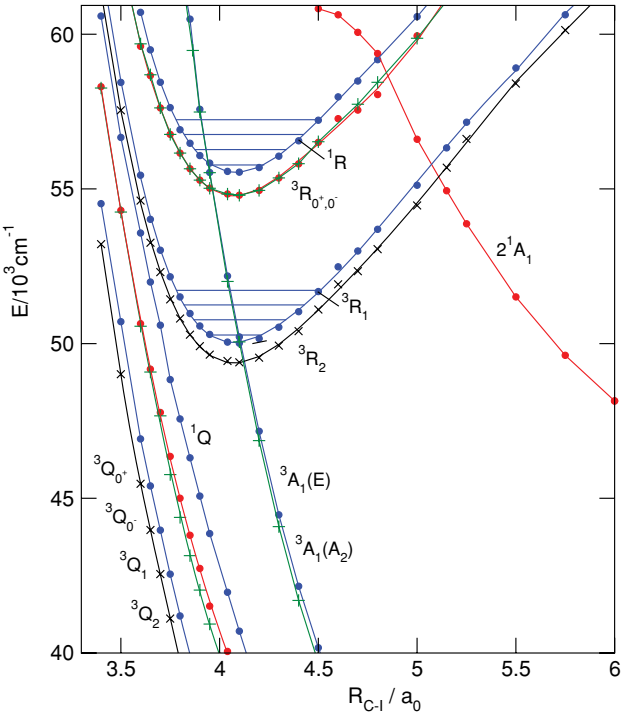

FIG. 2. Calculated potential energy curves for the excited states of CH_3I relevant to the B- and C-band absorption and predissociation. The $C_{\infty v}$ group notation is used. The $\Omega = 0^+$ states are shown in red, $\Omega = 0^-$—in green, $\Omega = 1$—in blue, and $\Omega = 2$—in black (see text). The lowest four vibrational levels are shown for the $^3R_1$ and ^1R states.

The calculated spectroscopic constants for the five lowest Rydberg states are given in Table II together with the vertical excitation energies for the repulsive $^3A_1(A_2, E)$ states. One can see that potential minima for all Rydberg states occur at nearly the same equilibrium geometries, $R_{C-I} = 4.079 - 4.085\ a_0$ and $\alpha = 115.0°$, which differ only slightly from that for the CH_3I ground state, $R_{C-I} = 4.04\ a_0$, $\alpha = 111.0°$. This shows that the n MO, with its predominantly iodine $5p$ character, is essentially nonbonding for this system. The computed T_e values for the $^3R_2$ and $^3R_1$ states are 49 398 and 50 010 cm^{-1}, respectively, and are thus in very good agreement with the T_0 values of 49 220 and 49 710 cm^{-1} determined by Felps *et al.*[6] Agreement with experiment is slightly

TABLE II. Calculated and experimental spectroscopic constants (transition energies T_e, bond lengths R_e, and vibrational frequencies ν_3) for the lowest Rydberg states of CH_3I. All values given without references are obtained in the present study. The vertical excitation energies for the repulsive $^3A_1(A_2, E)$ states are calculated at $R_e(\tilde{X}\ ^1A_1) = 4.04$ a_0.

	T_e (cm^{-1})		ν_3(cm^{-1})		R_e (a_0)
State	Calc.	Exp.[a]	Calc.	Exp.[a]	Calc.
$^3R_2(E)$	49 398	49 220	482		4.083
$^3R_1(E)$	50 010	49 710	492	485	4.087
$^3R_{0^-}(A_2)$	54 790		481		4.079
$^3R_{0^+}(A_1)$	54 792	54 040	481		4.079
$^1R_1(E)$	55 549	54 625	483	470	4.085
$^3A_1(A_2)$	52 009				
$^3A_1(E)$	52 187				

[a] T_0 values from Ref. 6.

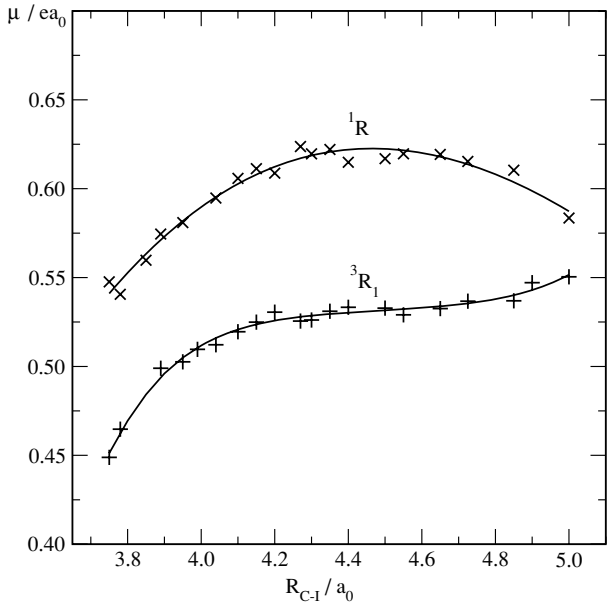

FIG. 3. Calculated electric-dipole moments for the perpendicular $^3R_1, ^1R(E) \leftarrow \tilde{X}\,A_1$ transitions. The symbols show the calculated points and the curves correspond to polynomial fits.

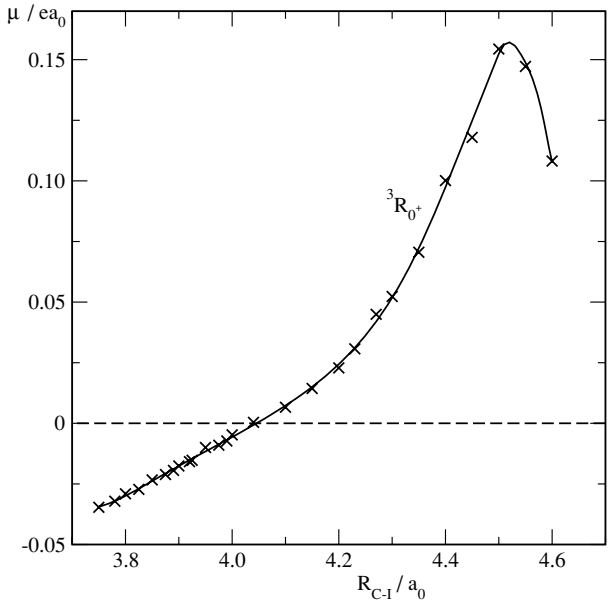

FIG. 4. Calculated electric-dipole moment for the parallel $^3R_{0^+}(A_1) \leftarrow \tilde{X}\,A_1$ transitions. The crosses are the calculated points and the curve is the polynomial fit.

worse for the $^3R_{0^+}$ and ^1R states, but still remains reasonably good. The calculated ν_3 frequencies for the C–I stretching vibration for the five lowest Rydberg states lie in the $481 - 492$ cm^{-1} interval and are slightly smaller than that ($\nu_3 = 524$ cm^{-1}) of the $\tilde{X}\,A_1$ ground state. Comparison with experiment, which is possible only for the $^3R_1$ and ^1R states, finds good agreement between the measured and calculated ν_3 values (see Table II).

B. Transition moments and absorption in the *B* and *C* bands

The computed electric dipole moments for the perpendicular $^3R_1, ^1R(E) \leftarrow \tilde{X}A_1$ and parallel $^3R_{0^+}(A_1) \leftarrow \tilde{X}A_1$ transitions are shown in Figs. 3 and 4, respectively. As described in Sec. II, they have been calculated employing the LSC–SO–CI method for a large number of $\Lambda - S$ roots (17–18 per symmetry) because contributions of the higher-lying roots are non-negligible, particularly in the $^3R_{0^+} \leftarrow \tilde{X}$ case. One can see that transition moment values μ for the perpendicular $^3R_1, ^1R \leftarrow \tilde{X}$ transitions are fairly large and lie in the 0.45–0.62 ea_0 range. At the ground state equilibrium geometry, the computed μ values for the $^3R_1 \leftarrow \tilde{X}$ and $^1R \leftarrow \tilde{X}$ transitions are 0.512 and 0.595 ea_0, respectively. From the analysis of the corresponding wave functions it is clear that the main contribution to both transitions comes from the allowed $^1R(^1E) \leftarrow \tilde{X}\,^1A_1$ transition. Since the direct SO coupling between the ^3R and ^1R states is very strong (2682 cm^{-1} at $R_{C-I} = 4.04\ a_0$), the corresponding transition moments have comparable values, though the transition to the higher-lying singlet state is always stronger.

The parallel $^3R_{0^+}(A_1) \leftarrow \tilde{X}$ transition moment is much smaller than those for the perpendicular transitions, particularly in the center of the FC region. This transition is spin-forbidden and becomes allowed mainly due to the SO coupling with the $\tilde{X}\,^1A_1$ and $2\,^1A_1$ singlet states. The latter states lie far away from $^3R(^3E)$ in the middle of the FC region, which explains the weakness of the $^3R_{0^+} \leftarrow \tilde{X}$ transition. Another important finding of this study is that the contributions of the above states to the $\mu(^3R_{0^+} \leftarrow \tilde{X})$ transition moment have opposite signs, which leads to a node in the $\mu(R_{C-I})$ function. It occurs very close to the equilibrium geometry of the ground state (see Fig. 4) and provides an additional reason why the $^3R_{0^+} \leftarrow \tilde{X}$ transition is weak. At larger internuclear distances the $^3R_{0^+} \leftarrow \tilde{X}$ transition moment increases since the $2\,^1A_1$ contribution gradually begins to dominate as the ^3R and $2\,^1A_1$ states come closer (see Fig. 2). This has, however, only a very small effect on absorption to the lowest vibrational levels of the $^3R_{0^+}(A_1)$ state.

The B absorption band is composed of transitions to the $^3R_2(E)$ and $^3R_1(E)$ states, with clear domination of the latter. The $^3R_2(E) \leftarrow \tilde{X}A_1$ transition, though formally allowed in the C_{3v} group, is much weaker, since it corresponds to a $\Delta\Omega = 2$ transition in the $C_{\infty v}$ symmetry. The $\mu(^3R_2 \leftarrow \tilde{X})$ values computed in this work lie in the $(1 - 3) \times 10^{-3}$ ea_0 interval. These data cannot be considered to be very accurate, however, since they exhibit rather strong and irregular variation when the size of the SO matrix is increased. Nevertheless, the data are reliable enough to conclude that this transition moment is significantly ($10^2 - 10^3$ times) smaller than the $^3R_1 \leftarrow \tilde{X}$ one, at least when no strong bending of the CH_3I molecule is involved.

The situation with absorption in the C band is qualitatively similar. There are two allowed electronic transitions in this spectral range, $^3R_{0^+}(A_1), ^1R(E) \leftarrow \tilde{X}A_1$, but the perpendicular transition clearly dominates the C band. This result is not *a priori* as obvious as for the B band, but follows from the accurate *ab initio* calculations. In this connection, it is also worth noting that the situation in the A absorption band is

opposite, with the parallel $^3Q_{0^+}(A_1) \leftarrow \tilde{X}A_1$ transition being notably stronger than $^1Q(E) \leftarrow \tilde{X}A_1$.[5]

The transition moment data obtained in this work allow one to calculate radiative lifetimes for the electronic states discussed. The calculated values for the lowest vibrational level ($\nu_3 = 0$) in the $^3R_1$ and ^1R states are 14.7 and 8.0 ns, respectively. This shows that the radiative depopulation of these states is quite efficient, but still about 10^3 times slower than the predissociation process, which is characterized by lifetimes ~ 1 ps.[8,14]

From the above discussion it is clear that both the B and C absorption bands are characterized by the perpendicular polarization which leads to the corresponding anisotropy in the angular distribution of the dissociation products. Perpendicular polarization of the B absorption band has also been found experimentally by van Veen *et al.*,[9] who measured the β anisotropy parameter to be -0.72 ± 0.1, and this finding has been confirmed in the later experimental studies.[10,14,17] In the very recent femtosecond velocity map imaging study,[14] it has been directly demonstrated that at the early product detection times, $\beta = -1$, as expected for a purely perpendicular transition. The deviation from the limiting $\beta = -1$ value can be explained by the CH_3I molecule rotation following excitation, but prior to dissociation. As has been shown by Gilchrist *et al.*,[17] this effect can be quantified by employing the β formula of Bush and Wilson,[31] which takes into account rotation of the parent molecule during dissociation of an excited bound state. Thus calculated β value of -0.76 (Ref. 17) is in very close agreement with the experimental result of Ref. 9.

C. Predissociation in the *B* and *C* bands

Analysis of the possible predissociation mechanisms for the bound states belonging to the B and C bands is of special interest for the present study. From the potential energy data calculated in this work (see Fig. 2), it unambiguously follows that the repulsive E, $A_2(^3A_1)$ states, which cross the B- and C-band states near their minima, provide the main channels for their predissociation. As discussed in Sec. III A, the SO splitting between the $A_2(^3A_1)$ and $E(^3A_1)$ states is very small since they correspond to the $\Omega = 0^-, 1$ components of the $^3\Sigma^+$ state in $C_{\infty v}$. From symmetry considerations, it is however clear that the main decay channel for the $^3R_2$, $^3R_1$, ^1R states of E symmetry is the $^3A_1(E)$ state, and it is the SO coupling which causes their predissociation.

Wang *et al.*[20] in their very recent study, as well as Syage[11] earlier, have interpreted their experimental data on the basis of the early theoretical analysis.[18,19] These authors have concluded that the $\tilde{B}\,2$ and $\tilde{C}\,2$ states (the $\tilde{B}\,2$ and $\tilde{C}\,2$ notations have been used for $^3R_1$ and ^1R as second absorbing state of each band, respectively) are predissociated by the A_2 component of the $^3Q_0$ state ($^3Q_{0^-}$). The present *ab initio* calculations clearly show that the $^3Q_{0^-}$ state lies much lower in energy than all the B- and C-band states (see Fig. 2) and thus cannot be responsible for their decay in the FC region.

Both decay channels discussed lead to formation of the spin-excited $I(^2P_{1/2})$ atoms. So, it is important to answer the question of how (if at all) the ground state $I(^2P_{3/2})$ atoms could be obtained from the CH_3I photodissociation in the B band, as has been found in Ref. 16 for excitation at 193 nm. The only feasible explanation seems to be the predissociation of the B-band states through their interaction with the repulsive $^1Q(E)$ state, which may occur at the repulsive limbs of the bound states. As can be seen from Fig. 2, however, such an interaction comes into play only at relatively high excitation energies $\geq 55\,000$ cm^{-1} and no detailed experimental study has been undertaken until now to analyze this possibility. Such vertical excitation energies correspond to $R_{C-I} \leq 3.6$ a_0, where the corresponding direct SO coupling between the $^1Q(E)$ and $^3R_1(E)$ states is relatively strong, 360 cm^{-1} at $R_{C-I} = 3.6\,a_0$. So it may be interesting to look for the ground state $I(^2P_{3/2})$ atoms as photodissociation products at the excitation wavelength of ≈ 180 nm. This effect may be masked, however, by the strong absorption to the $^1R(E)$ state, with the 0_0^0 band origin lying at 183.1 nm. Therefore, this problem may be a real challenge for experimentalists. It is important to underline that the $^1Q(E)$ decay channel does not play any role at the excitation wavelength of 193 nm, and the $I(^2P_{3/2})$ atoms detected by Hess *et al.*[16] most probably come from the simultaneous molecular iodine dissociation discussed in Ref. 17. The other A-band states lie notably lower in energy in the FC region and their influence on the predissociation of the B- and C-band states is negligible.

There is one more problem concerning the B-band photodissociation which is interesting to analyze on the basis of the present *ab initio* data. It is known from the experiment (see, e.g., Ref. 8) that all the vibrationally excited states have lifetimes that differ from that of the vibrationless level. Wang and Ziegler[32] have found that the predissociation of the $^3R_1(E)$ state ($\tilde{B}\,2$ in their notation) becomes slower upon excitation of the ν_3 C–I stretching mode. This finding has later been confirmed by Baronavski and Owrutsky,[8] who measured the predissociation lifetime to increase three times when going from 0_0^0 to 3_0^1. This result contradicts the conclusions from the previous spectroscopic studies[18,33] and seems to be counterintuitive at first glance. In the axial-recoil approximation, the C–I coordinate is the dissociation coordinate, so that excitation of the ν_3 mode should enhance dissociation and reduce the lifetime. On the basis of the present calculations, this effect finds a simple and natural explanation. It can be seen from Fig. 2 that the $^3A_1(E)$ repulsive state crosses $^3R_1(E)$ very close to the equilibrium C–I distance of the latter. Hence, it is clear that the coupling matrix element over the corresponding vibrational functions must be significantly larger in the case of $\nu_3 = 0$ relative to the $\nu_3 = 1$ level, and this leads to the notably shorter lifetime of the former.

Vaida and co-workers[33,34] and Baronavski and Ovrutsky[8] have also reported an enhanced rate of predissociation of the $\tilde{B}2\,(^3R_1)$ state when the ν_6 bending mode is excited. On the basis of the present calculated data, this experimental result may be explained by the lower CH_3I molecular symmetry (C_s) in this case, which opens an additional dissociation channel, namely, through coupling with the $^3A_1(A_2)$ state transforming according to A'' IR in the C_s group, while all Rydberg states of E symmetry are split into the A' and A'' components. Alternatively, one can speak about vibronic

coupling with the ν_6 vibration of e symmetry, which produces $E \otimes e = A_1 + A_2 + E$ vibronic states.

The opening of the $^3A_1(A_2)$ channel must also enhance the predissociation of the $^3R_2(E)$ state, but the $^3R_2(E)$ coupling with both the $^3A_1(E, A_2)$ states is significantly weaker. This can be better understood in the $C_{\infty v}$ group, which can be considered as a fairly accurate approximation for the axial CH_3–I recoil. In the $C_{\infty v}$ symmetry, this interaction corresponds to the $\Omega = 2$ coupling with the $\Omega = 1$ and 0^- states and thus must necessarily involve rotation in order to be allowed. In C_{3v} and C_s groups such coupling is no longer forbidden, but remains quite weak in comparison with the allowed $\Omega = 1 \leftrightarrow \Omega = 1$ interaction.

Predissociation in the C band is qualitatively similar to that in the B band. The $^3A_1(E)$ state is mainly responsible for the decay of the $^1R(E)$ ($\tilde{C}$ 2) state dominating the C-band absorption. The other C-band state, $^3R_{0^+}(A_1)$, has different symmetry than the repulsive states, which means that ν_6 or any other asymmetric mode must be involved to make the dissociation process allowed. Depopulation of the $^3R_{0^+}(A_1)$ state may also occur due to its crossing with the $A_1(^1\Sigma^+)$ valence state which has a lower minimum than that of the $^3R_{0^+}$ state and converges to the excited CH_3 limit (see Fig. 2).

IV. CONCLUSION

Multireference spin–orbit CI calculations have been carried out for the valence and low-lying Rydberg states of CH_3I responsible for the B and C absorption bands. Potential energy surfaces along the C–I dissociation coordinate (minimal energy paths with respect to the umbrella angle) have been obtained as well as transition moments for excitation of the Rydberg states. The calculated *ab initio* data have been used to analyze absorption in the B and C bands and predissociation of the corresponding states.

It is shown that the B and C bands are dominated by the perpendicular $^3R_1(E) \leftarrow \tilde{X}\,A_1$ and $^1R(E) \leftarrow \tilde{X}\,A_1$ transitions, respectively, which results in the perpendicular anisotropy of the dissociation product angular distribution observed experimentally.[9,14] It is also found that the parallel $^3R_{0^+}(A_1) \leftarrow \tilde{X}\,A_1$ transition belonging to the C band is very weak due to the node in the $\mu(R_{C-I})$ function calculated to occur close to the ground state equilibrium geometry.

From the PES data obtained in this study, it clearly follows that the bound Rydberg states of the B and C bands are predissociated due to the coupling with the repulsive E and A_2 components of the $^3A_1$ state, weakly split by the spin–orbit interaction. For reasons of symmetry, the coupling with the $^3A_1(E)$ state must dominate predissociation in both absorption bands. Both decay pathways discussed converge to the $CH_3 + I(^2P_{1/2})$ dissociation limit. It is predicted that the only feasible way to obtain the $I(^2P_{3/2})$ ground state atoms from the CH_3I photodissociation in the B band is through interaction of the $^3R_1(E)$ state with the repulsive $^1Q(E)$ valence state, but this process only becomes efficient at excitation energies $\geq 55\,000\ cm^{-1}$.

The calculations show further that the conical intersection of the repulsive $^3A_1$ state with the $^3R_1(E)$ state responsible for the B-band absorption takes place close to the equilibrium geometry of the latter. This explains the experimental finding[8,32] that excitation of the ν_3 stretching mode (3_0^1) leads to a larger predissociation lifetime than that for the vibrationless level. This effect is caused by the significantly smaller overlap of the corresponding vibrational wave functions.

Excitation of the bending ν_6 mode lowers the molecular symmetry and thus leads to the opening of the additional $^3A_1(A'')$ decay channel, which enhances the predissociation rates. A more detailed analysis of the predissociation process requires elaborate calculations of the multidimensional PESs and nonadiabatic coupling matrix elements and such calculations are in progress now.

ACKNOWLEDGMENTS

We would like to express our gratitude to the Deutsche Forschungsgemeinschaft for its financial support in the framework of Project BU 450/21-2.

[1] A. T. J. B. Eppink and D. H. Parker, J. Chem. Phys. **109**, 4758 (1998); *ibid.* **110**, 832 (1999).
[2] R. de Nalda, J. Dura, A. García-Vela, J. G. Izquierdo, J. Gonzalez-Vazquez, and L. Bañares, J. Chem. Phys. **128**, 244309 (2008).
[3] L. Rubio-Lago, A. García-Vela, A. Arregui, G. A. Amaral, and L. Bañares, J. Chem. Phys. **131**, 174309 (2009).
[4] A. B. Alekseyev, H.-P. Liebermann, R. J. Buenker, and S. N. Yurchenko, J. Chem. Phys. **126**, 234102 (2007).
[5] A. B. Alekseyev, H.-P. Liebermann, and R. J. Buenker, J. Chem. Phys. **126**, 234103 (2007).
[6] S. Felps, P. Hochmann, P. Brint, and S. P. McGlynn, J. Mol. Spectrosc. **59**, 355 (1976).
[7] J. D. Scott, W. S. Felps, G. L. Finley, and S. P. McGlynn, J. Chem. Phys. **68**, 4678 (1978).
[8] A. P. Baronavski and J. C. Owrutsky, J. Chem. Phys. **108**, 3445 (1998).
[9] G. N. A. van Veen, T. Baller, and A. E. de Vries, Chem. Phys. **97**, 179 (1985).
[10] R. E. Continetti, B. A. Balko, and Y. T. Lee, J. Chem. Phys. **89**, 3383 (1988).
[11] J. A. Syage, Chem. Phys. Lett. **212**, 124 (1993).
[12] P. G. Wang, Y. P. Zhang, C. J. Ruggles, and L. D. Ziegler, J. Chem. Phys. **92**, 2806 (1990); L. D. Ziegler, Y. C. Chung, P. G. Wang, and Y. P. Zhang, J. Phys. Chem. **94**, 3394 (1990).
[13] M. H.M. Janssen, M. Dantus, H. Guo, and A. H. Zewail, Chem. Phys. Lett. **214**, 281 (1993).
[14] G. Gitzinger, M. E. Corrales, V. Loriot, G. A. Amaral, R. de Nalda, and L. Bañares, J. Chem. Phys. **132**, 234313 (2010).
[15] N. Thiré, R. Cireasa, V. Blanchet, and S. T. Pratt, Phys. Chem. Chem. Phys. **12**, 15644 (2010).
[16] W. P. Hess, R. Naaman, and S. R. Leone, J. Phys. Chem. **91**, 6085 (1987).
[17] A. Gilchrist, G. Hancock, R. Peverall, G. Richmond, G. A.D. Ritchie, and S. Taylor, J. Phys. Chem. A **112**, 4531 (2008).
[18] D. J. Donaldson, M. S. Child, and V. Vaida, J. Chem. Phys. **88**, 7410 (1988).
[19] M. Tadjeddine, J. P. Flament, and C. Teichteil, Chem. Phys. **118**, 45 (1987).
[20] Y. Wang, H. Shen, L. Hua, C. Hu, and B. Zhang, Opt. Express **17**, 10506 (2009).
[21] A. B. Alekseyev, H.-P. Liebermann, D. B. Kokh, and R. J. Buenker, J. Chem. Phys. **113**, 6174 (2000).
[22] L. A. LaJohn, P. A. Christiansen, R. B. Ross, T. Atashroo, and W. C. Ermler, J. Chem. Phys. **87**, 2812 (1987).
[23] M. Glukhovtsev, A. Pross, M. P. McGrath, and L. Radom, J. Chem. Phys. **103**, 1878 (1995).
[24] T. H. Dunning, Jr, J. Chem. Phys. **90**, 1007 (1989).
[25] R. J. Buenker and S. D. Peyerimhoff, Theor. Chim. Acta **35**, 33 (1974); *ibid.* **39**, 217 (1975); R. J. Buenker, S. D. Peyerimhoff, and W. Butscher, Mol. Phys. **35**, 771 (1978).

[26]R. J. Buenker and R. A. Phillips, J. Mol. Struct.: THEOCHEM **123**, 291 (1985).
[27]S. Krebs and R. J. Buenker, J. Chem. Phys. **103**, 5613 (1995).
[28]E. R. Davidson, in *The World of Quantum Chemistry*, edited by R. Daudel and B. Pullman (Reidel, Dordrecht, 1974), p. 17.
[29]G. Hirsch, P. J. Bruna, S. D. Peyerimhoff, and R. J. Buenker, Chem. Phys. Lett. **52**, 442 (1977); D. B. Knowles, J. R. Alvarez-Collado, G. Hirsch, and R. J. Buenker, J. Chem. Phys. **92**, 585 (1990).
[30]A. B. Alekseyev, H.-P. Liebermann, and R. J. Buenker, in *Recent Advances in Relativistic Effects in Chemistry*, edited by K. Hirao and Y. Ishikawa (World Scientific, Singapore, 2003), p. 65.
[31]G. E. Bush and K. R. Wilson, J. Chem. Phys. **56**, 3638 (1972).
[32]P. G. Wang and L. D. Ziegler, J. Chem. Phys. **95**, 288 (1991).
[33]D. J. Donaldson, V. Vaida, and R. Naaman, J. Chem. Phys. **87**, 2522 (1987); J. Phys. Chem. **92**, 1204 (1988).
[34]S. P. Sapers, V. Vaida, and R. Naaman, J. Chem. Phys. **88**, 3638 (1988).